

Fly Your Satellite!

Analysis Report (ARPT)

Attitude and Orbit Control System (AOCS)



UNIVERSITAT POLITÈCNICA
DE CATALUNYA
BARCELONATECH

NANOSAT LAB



FLY YOUR SATELLITE!

Contents

1	Introduction	9
1.1	The PoCat-Lektron mission	9
1.1.1	Mission statement	9
1.1.2	Mission Objectives	9
2	Simulation model	10
2.1	PocketQube Model	10
2.2	Software and hardware delays	10
2.3	Environmental model and assumptions	10
2.3.1	Reference frames	10
2.3.2	Environmental models	12
2.3.3	External disturbances	12
2.4	Orbit and attitude kinematic propagators	12
2.5	Sensor and actuator models	13
2.5.1	Gyroscope	13
2.5.2	Photodiodes	13
2.5.3	Magnetometer	13
2.5.4	Magnetorquer	14
2.6	Simulaton / model sampling times and frequencies	14
3	Simulation performance campaign plan and results	14
3.1	Nadir Pointing Mode	14
3.1.1	Assumptions and limitations	14
3.1.2	Nadir pointing results	15
3.1.3	Nadir pointing using an Extended Kalman Filter (EKF) for attitude determination	21
3.2	Detumbling mode	30

Acronyms

AOCS Attitude and Orbit Control System

APE Absolute Performance Error

CS Cubesat

ECI Earth Centered Inertial

EKF Extended Kalman Filter

FSS Federated Satellite System

FYS Fly Your Satellite!

LVLH Local Vertical Local Horizontal

OBC On Board Computer

OPQK IEEE OpenPocketQube Kit

PNT Position Navigation and Timing

PQ PocketQube

PT Princeton Toolbox

RFI Remote Frequency Interference

UPC NL UPC NanoSat Lab

List of Figures

2.1	PQ 3D model	10
2.2	ECI frame representation	11
2.3	Body frame representation	11
2.4	LVLH frame representation	12
3.1	Ground track of the simulated PQ orbit	15
3.2	Eclipse phases	15
3.3	Drag Force (mN)	16
3.4	Radiation Force (mN)	16
3.5	Aerodynamic Torques	16
3.6	Gravity Gradient Torques	16
3.7	Radiation Torques	16
3.8	Gyro data X Axis	17
3.9	Gyro data Y Axis	17
3.10	Gyro data Z Axis	17
3.11	Magnetometer data X Axis	17
3.12	Magnetometer data Y Axis	17
3.13	Magnetometer data Z Axis	17
3.14	Photodiode data	17
3.15	Sun position (ECI) X Axis	18
3.16	Sun position (ECI) Y Axis	18
3.17	Sun position (ECI) Z Axis	18
3.18	Magnetic Field (ECI Frame)	18
3.19	Attitude Rate	19
3.20	Magnetic torque	19
3.21	Intensity x Axis	20
3.22	Intensity y Axis	20
3.23	Intensity z Axis	20
3.24	LVLH To Body Quaternion	20
3.25	Angle between nadir and +Y	21
3.26	Angle between nadir and +Y with delay	21
3.27	Drag Force (mN)	22
3.28	Radiation Force (mN)	22
3.29	Aerodynamic Torques	22
3.30	Gravity Gradient Torques	22
3.31	Radiation Torques	23
3.32	Gyro data X Axis	23
3.33	Gyro data Y Axis	23
3.34	Gyro data Z Axis	23
3.35	Magnetometer data X Axis	23
3.36	Magnetometer data Y Axis	23
3.37	Magnetometer data Z Axis	23
3.38	Photodiode data	24
3.39	Sun position (ECI) X Axis	24
3.40	Sun position (ECI) Y Axis	24
3.41	Sun position (ECI) Z Axis	24
3.42	Attitude Rate	25
3.43	Magnetic Torques	25
3.44	Intensity x Axis	25
3.45	Intensity y Axis	25
3.46	Intensity z Axis	25
3.47	LVLH To Body Quaternion	26
3.48	LVLH To Body Quaternion	26
3.49	LVLH To Body Quaternion	27
3.50	Quaternion evolution for 20 simulations	28
3.51	Performance q_1	28
3.52	Performance q_2	29

3.53 Performance q_3	30
3.54 Performance q_4	30

List of Tables

APPROVAL

Title FYS DRD and Guidelines			
Issue Number	1	Revision Number	0
Author	Edgar Hernandez Recio	Date	
Approved By		Date of Approval	

CHANGE LOG

Reason for change	Issue Nr	Revision Number	Date
First release	1	0	
Second release	2	0	

CHANGE RECORD

Issue Number	Revision Number		
Issue Number	1	Revision Number	0
Reason for change	Date	Pages	Paragraph(s)
First release			
Second release			

DISTRIBUTION

Disclaimer

This document has been prepared for use by the Fly Your Satellite! PoCat Lektron team.

**This document shall be considered confidential and not to be distributed further without permission of
ESA Education, and the authors.**

1 Introduction

The ^{Po}Cat-Lektron Attitude and Orbit Control System (AOCS) analysis includes a comprehensive simulation model to support the design, verification, and validation of the AOCS for the ^{Po}Cat-Lektron mission. Developed at the UPC NanoSat Lab (UPC NL) as part of the IEEE OpenPocketQube Kit (OPQK) initiative and selected for the ESA Fly Your Satellite! (FYS) program, the mission comprises two 1P PocketQubes (PQ) equipped with L-band and K-band radiometers for remote sensing and Remote Frequency Interference (RFI) monitoring.

The simulation campaign evaluates key operational modes, such as Nadir Pointing and Detumbling, assessing performance against mission requirements. Results demonstrate the impact of sensor noise and external disturbances, and highlight the effectiveness of advanced estimation techniques like the Extended Kalman Filter (EKF) in improving attitude determination and meeting pointing accuracy objectives. This simulation framework provides critical insights for the successful implementation of the AOCS in the ^{Po}Cat-Lektron.

1.1 The ^{Po}Cat-Lektron mission

1.1.1 Mission statement

The ^{Po}Cat-Lektron is a mission resulting from the OPQK initiative, developed at the UPC NL. The mission has been selected in the 4th call of the ESA FYS program. The mission analysis presented corresponds to the ^{Po}Cat-Lektron mission. It consists of two 1P PQs, the PoCat-2 and the PoCat-3, developed as a part of the OPQK. This mission aims to demonstrate the feasibility of PQ platforms for remote sensing applications.[?]

The payloads on board of the PQs are two passive radiometers to be used for RFI purposes on K and L bands. Apart from the remote sensing nature of the mission, this mission also aims to demonstrate the feasibility of the PQ platforms to create, manage and join Federated Satellite Systems (FSS). To do so, the FSS Experiment will be reproduced as a part of the experiments of the mission.

1.1.2 Mission Objectives

- **Demonstration of Scientific Viability:** Demonstrate the feasibility of conducting scientific missions using PQ platforms. To do so, the mission proposes collecting valuable RFI data through a K-Band and L-Band passive radiometers (One for each PQ). The payloads will monitor interferences on these bands. This data will facilitate enhanced detection and the generation of heatmaps indicating RFI distribution across the globe. In this experiment we aim to obtain data on the K-Band to see the impact on the atmospheric water vapor measurements, and in the L-Band the interferences over the Position Navigation and Timing (PNT) signals.
- **Satellite Federation Concept:** To establish and demonstrate that PQ platforms can create, manage and join FSS. This proof of concept for this resource-limited platforms is based on the reproduction of the FSS Experiment conducted at the UPC NL. The demonstration consists on creating a federation between 2 PQs, in order to download data. Previous missions such as the FSS-Cat from the UPC NL demonstrated the feasibility of this opportunistic collaboration using 6U CubSats (CS).
- **Educational Development:** As a mission developed at the UPC NL, the mission is oriented for undergraduate students to gain experience and get involved in real space missions. In addition, several Bachelor and Master Thesis had been done from this project, apart from the academic papers that this project has produced.

2 Simulation model

To verify the Attitude and Orbit Control System (AOCS) design, verification and validation, a simulation model using matlab code has been used. The simulation is based on the Princeton Toolbox (PT) [1], which contains a set of functions and simulations initially created for CubeSats, that has been adapted to the PocketQube (PQ).

2.1 PocketQube Model

To model the PQs of the mission, a 3 dimensional cube has been used as a geometric representation, as shown in *Figure 2.1*. This cube has the same dimensions as a PQ $5 \times 5 \times 5 \text{ cm}^3$ and the same mass as the PQs. Additionally, as the mission is formed by two PQs, in order to create them as close as possible to the reality the inertia matrix is taken into account in the simulation.

The satellites will be simulated in two different configurations, on the one hand in stowed configuration (without the antennas deployed) and on the other hand in deployed configuration. In the case of the L-band PQ the stowed configuration contains both the L-band antenna and communications antenna stowed.

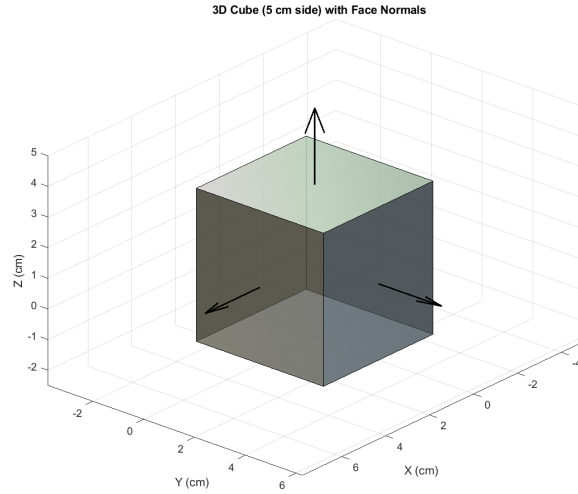


Figure 2.1: PQ 3D model

2.2 Software and hardware delays

In the report a simulation with a negligible delay is presented to show the performance of the Nadir pointing. Additionally, another simulation using a delay of 1 AOCS cycle is also presented so that the performance in a worse case scenario can be observed. This delay means that once the measurements of the sensors are obtained, they are not used until the next AOCS cycle, which in the case of the simulation is 1 second.

2.3 Environmental model and assumptions

2.3.1 Reference frames

- **Earth Centered Inertial (ECI) frame:**

The ECI frame is a global cartesian reference frame that has its origin at the centre of the Earth.

- X axis points to the Vernal Equinox.
- Y axis completes the set with the right-hand rule.
- Z axis aligned with the Earth's rotation axis.

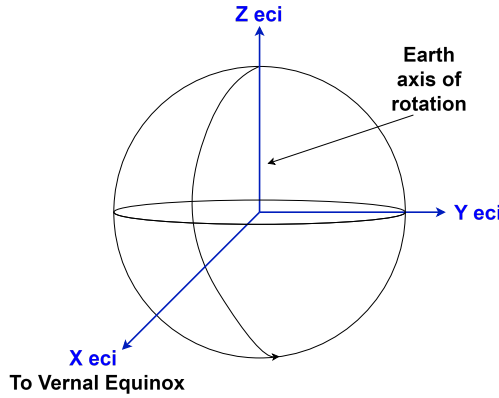


Figure 2.2: ECI frame representation

- **Body frame:**

The Body frame is a global cartesian reference frame that has its origin at the centre of the PQ.

- X axis aligned with the PQ width, parallel to the sliding plate and perpendicular to the direction of insertion into the PQ deployer.
- Y axis aligned with the PQ length, the direction of insertion into the PQ deployer and completing the right handed reference frame.
- Z axis aligned with the PQ height direction, pointing upwards from the sliding plate.

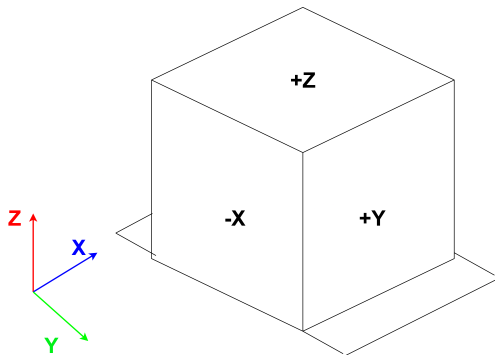


Figure 2.3: Body frame representation

- **Local Vertical Local Horizontal (LVLH) Frame:**

The LVLH Frame will be mainly used for results presentation in the Nadir pointing simulations. The frame is described as:

- X-Axis: Perpendicular to Y and Z, forming a right-handed coordinate system - Local Horizontal
- Y-Axis: Negative to the orbit normal, or in the direction of - \mathbf{h}
- Z-Axis: Oriented in the direction of $-\mathbf{r}$ (points to center of Earth) - Local Vertical

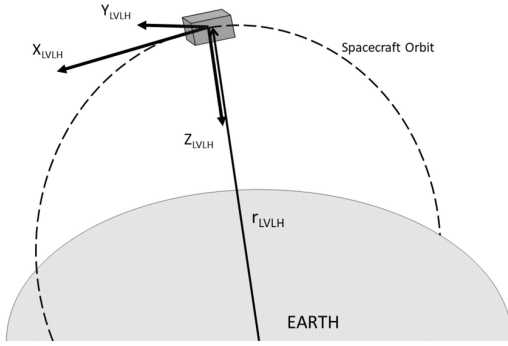


Figure 2.4: LVLH frame representation

2.3.2 Environmental models

The following environmental models are used in the simulation:

- **Earth's magnetic field model [2]:** The Earth's magnetic field model used in the simulation is based on the Tilted dipole mode, which includes the effect of the dipole motion of the Earth (the applied error of the model is also introduced).
- **Aerodynamic Drag model:** The simulation uses an aerodynamic drag model based on the Jacchia's 1970 model [3].
- **Radiation Pressure model:** The simulation includes the solar radiation pressure, the earth radiation pressure and the earth albedo pressure.
- **Gravity field model:** The simulation accounts for a point-mass gravity model.

2.3.3 External disturbances

The following external disturbances are considered in the simulation:

- **Drag force:**
- **Aerodynamic torques:**
- **Gravity gradient torques:**
- **Radiation Torques:**

2.4 Orbit and attitude kinematic propagators

As for the Orbit propagator in the simulation, firstly, the used equations of motion are the Cowell' form of the two body problem, using disturbances. In addition, the integrator type used is the Runge-Kutta 4th order method. As for the propagation of the parameters, they are done in the ECI frame.

The parameters included in the initial vector for describing the state of the satellite at the beginning of the simulation are:

- Satellite's position.
- Satellite's velocity.
- Satellite's attitude quaternion.
- Satellite's angular velocity.

Regarding the attitude representation of the satellite in the simulation, the mathematical expression that will be used is the quaternion. During the simulation the quaternion that will be used is the one representing the rotation from the body frame to the ECI frame. However, at the time to present the results the quaternion that will be used will be the one representing a rotation from the LVLH frame to the ECI frame.

2.5 Sensor and actuator models

In this section all the models used for the sensors and for the actuators are described. It is assumed that all the sensors have been calibrated and temperature characterized. A brief list of the sensors and actuators included in the PQ is presented below:

Sensors	Actuator
Gyroscope	Magnetorquer
Photodiodes	
Magnetometer	

2.5.1 Gyroscope

The model used to represent the gyroscope output given by [4] is:

$$\omega = \omega_o + b(t) + n, \quad (1)$$

where:

- ω is the measured angular velocity vector.
- ω_o is the true angular velocity of the satellite.
- b is the bias term, modeled as a random walk process.
- n is a zero-mean Gaussian noise vector.

2.5.2 Photodiodes

The output of the photodiodes can be modeled as:

$$v = v_o(T) + n \quad (2)$$

where:

- v is the measured voltage output vector,
- $v_o(T)$ is the true signal component that is dependent to the temperature T previously calibrated.
- n represents additive noise, typically modeled as zero-mean Gaussian noise.

2.5.3 Magnetometer

The magnetometer model is expressed as:

$$\mathbf{B}_{\text{meas}} = (\mathbf{C}_e \cdot \mathbf{B}_{\text{true}}) + \mathbf{b}_e + n \quad (3)$$

where:

- \mathbf{B}_{meas} is the measured magnetic field vector in the body frame.
- \mathbf{B}_{true} is the true magnetic field vector in the body frame.
- \mathbf{C}_e is the calibration matrix with errors.
- \mathbf{b}_e is the sensor bias error vector.
- n is zero-mean Gaussian white noise with known variance.

2.5.4 Magnetorquer

The magnetorquers are simulated as a mathematical formula. The magnetorquers generate a magnetic moment depending on the injected intensity, therefore, in the simulation this magnetic moment is calculated and later used to propagate the following attitude of the satellite with the other external disturbances. The formula used for calculating the magnetic moment generated by the magnetorquers is:

$$\mathbf{m} = I_o N_{layers} \sum_{i=1}^{N_{turns}} (l - 2(i-1)(w+d))^2 \quad (4)$$

Where the l is the length of the magnetorquer, the w the width of the copper trail, the d the distance between trails, N_{layers} is the number layers in which the magnetorquer is divided and N_{turns} is the number of turns in the magnetorquer. The I_o is the injected current, which is the input of the magnetorquer. The table below shows the characteristics of the magnetorquers used in the simulation:

Board	Turns	Max moment ($\text{A}\cdot\text{m}^2$)	Dimensions ($\text{mm} \times \text{mm}$)	Layers
Top	$42 \times \text{layer}$	9.17×10^{-4}	32×32	4
Bottom & Lateral	$38 \times \text{layer}$	0.0017	32×32	4

2.6 Simulator / model sampling times and frequencies

The simulation time used is 2 seconds which corresponds to 0.5 Hz. This is due to the fact that the On Board Computer (OBC) used in the PQ only has one thread to manage all the tasks, therefore, the sampling frequency has been chosen thinking in the worst case scenario. The sampling time of the sensors is the same one as the simulation time.

3 Simulation performance campaign plan and results

In this section the simulation results of the two different operational modes of the ADCS in the PQ are presented.

3.1 Nadir Pointing Mode

The objective of the Nadir Pointing is to point the Payload located at the top board of the PQ towards the Earth, so that the Payload can take measurements of the Earth. For this mode the following requirements have been defined:

The Absolute Performance Error (APE) of the Payload boresight shall be less than 20° with respect to the Y and X axes, which are the axes perpendicular to the boresight, and this requirement should be met for 95% of the time.

3.1.1 Assumptions and limitations

The list below presents the different assumptions and aspects considered to perform the simulations.

- Orbit parameters

- Inclination: 90 degrees
- Altitude: 500 Km
- Eccentricity: 0 degrees
- Initial satellite position: [6887 , 0 , 0] Km
- Initial satellite velocity: [0 , 0 , 7.6] Km/s

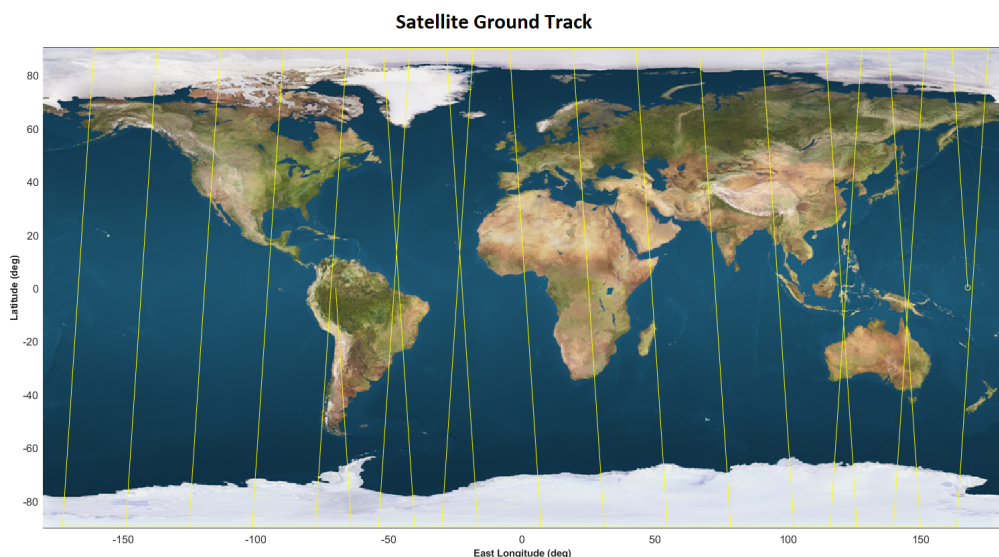


Figure 3.1: Ground track of the simulated PQ orbit



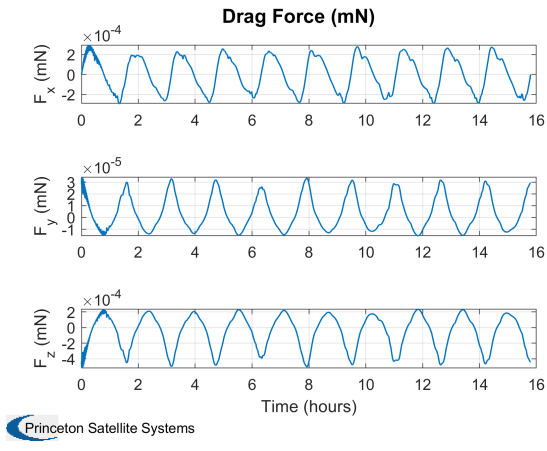
Figure 3.2: Eclipse phases

- **Number of simulated orbits:** 10 orbits
- **Simulation starting date:** 05/04/2027 00:00:00 UTC
- **Simulation time step:** 2 seconds

3.1.2 Nadir pointing results

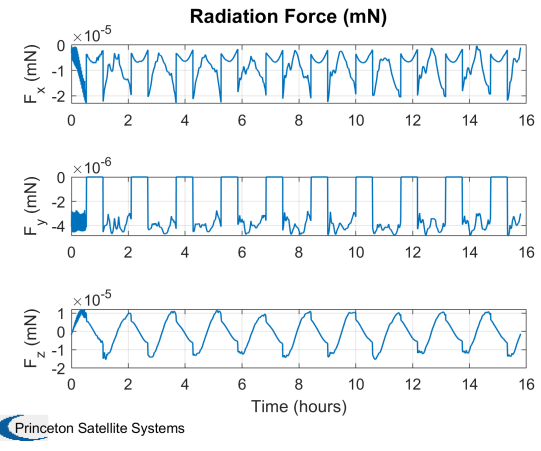
- **External perturbations**

In the following plots, the values of the different external perturbations affecting the simulation are shown.



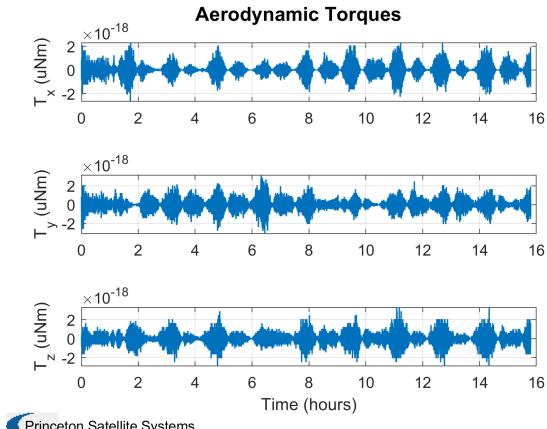
Princeton Satellite Systems

Figure 3.3: Drag Force (mN)



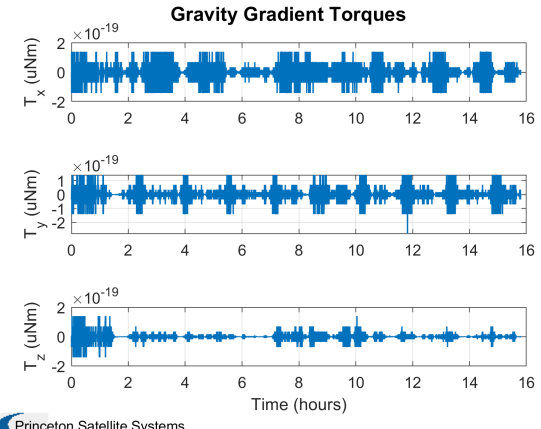
Princeton Satellite Systems

Figure 3.4: Radiation Force (mN)



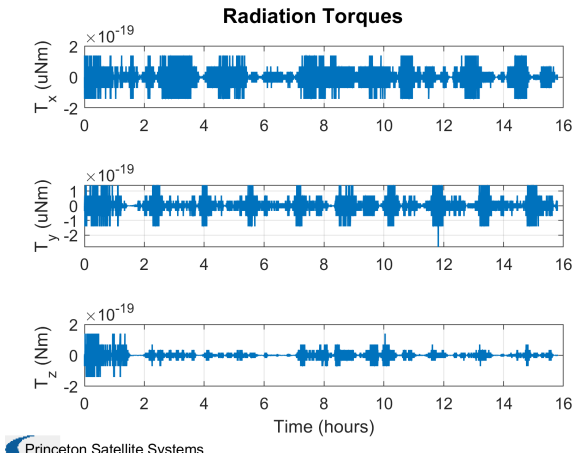
Princeton Satellite Systems

Figure 3.5: Aerodynamic Torques



Princeton Satellite Systems

Figure 3.6: Gravity Gradient Torques



Princeton Satellite Systems

Figure 3.7: Radiation Torques

• Sensor measurements

In this section the measures taken from the simulated sensors are presented. The sensors follow the model presented in the previous sections of the document. Firstly the measurements of the gyroscope are presented, it can be observed the effect that the noise and the random walk phenomenon has on the measures. It can also be observed how the Nadir Pointing controller first tries to conduct a little detumbling functionality in

order to reduce the angular velocity as much as possible. This effect can be observed in the first hour of the simulation.

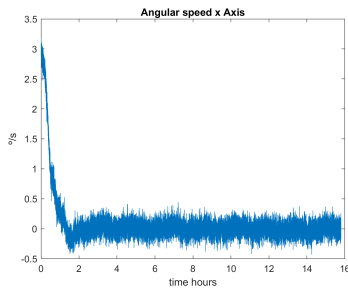


Figure 3.8: Gyro data X Axis

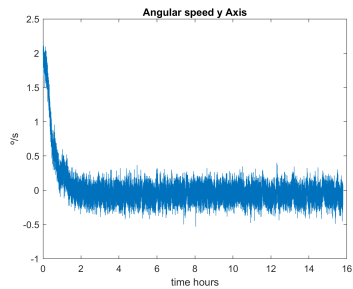


Figure 3.9: Gyro data Y Axis

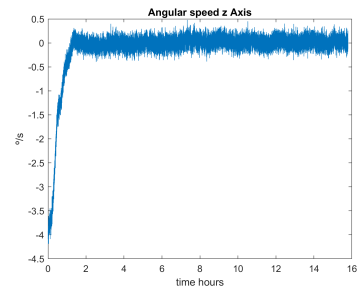


Figure 3.10: Gyro data Z Axis

Secondly, in the following pictures the magnetic field measured by the magnetometer is shown.

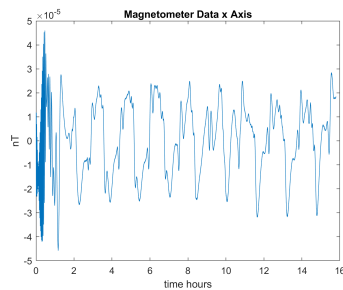


Figure 3.11: Magnetometer data X Axis

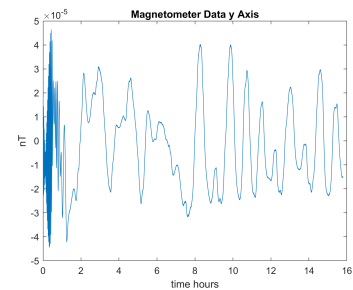


Figure 3.12: Magnetometer data Y Axis

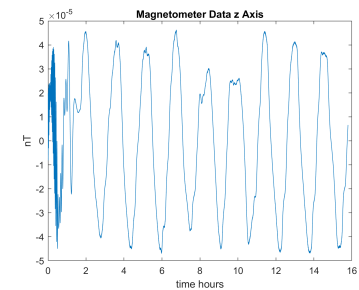


Figure 3.13: Magnetometer data Z Axis

Finally, the last plot of the sensors includes the measurements of all 6 photodiodes used in the satellite. Each axis of the PQ corresponds to the following number: 1 to $+Z$, 2 to $-Z$, 3 to $+X$, 4 to $+Y$, 5 to $-X$ and 6 to $-Y$.

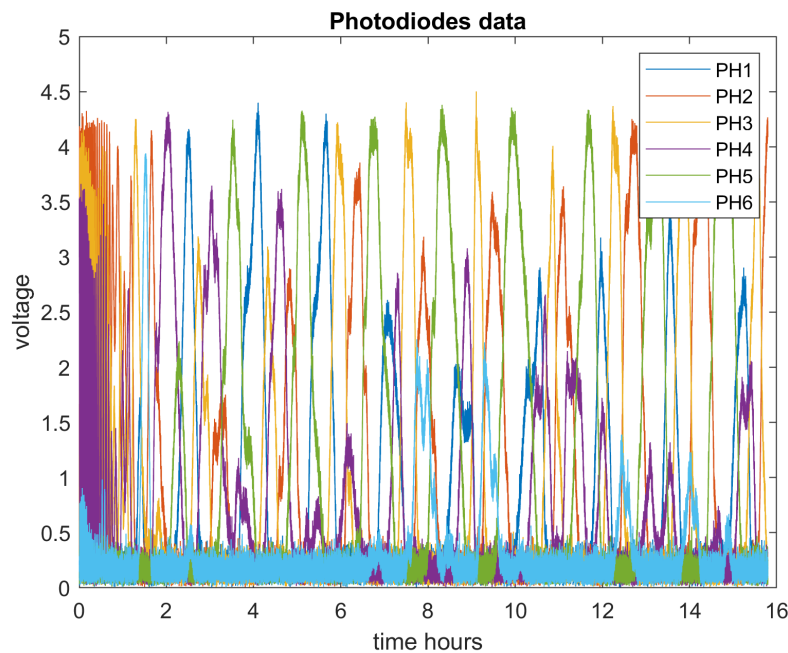


Figure 3.14: Photodiode data

- **Sun Position Algorithm Performance**

In the following section the performance of the developed Sun position algorithm estimator that uses the photodiodes and the temperature sensors is presented. The plots show two different lines, on the one hand an orange line which indicates the real position of the sun, and on the other hand a blue line which indicates the estimation of the algorithm. It can be observed that the performance of the estimation is degraded by the noise of the photodiodes, the less noise the better estimation.

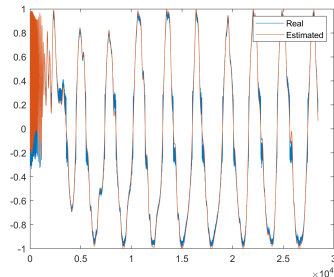


Figure 3.15: Sun position (ECI) X Axis

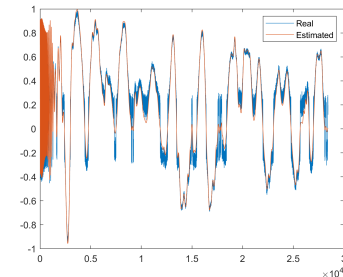


Figure 3.16: Sun position (ECI) Y Axis

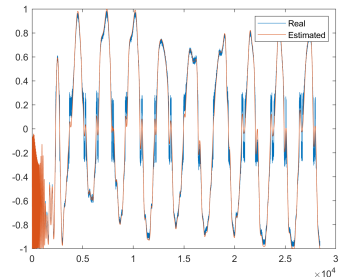


Figure 3.17: Sun position (ECI) Z Axis

- **Magnetic Field Model**

In this section the propagated magnetic field over the simulation is presented. The model as explained in the previous sections is based on the tilted dipole model to reduce as much as possible the simulation time.

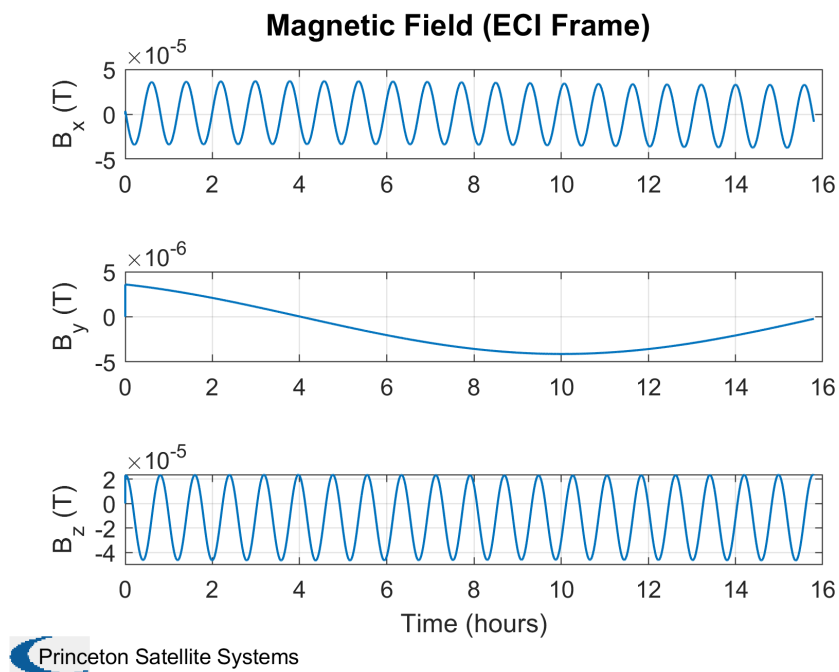


Figure 3.18: Magnetic Field (ECI Frame)

- **Real angular Velocity**

In the following plot it is shown the angular velocity propagated in each iteration of the simulation. In short words it is the real angular velocity in which the satellite is rotating due to the torques affecting the PQ.

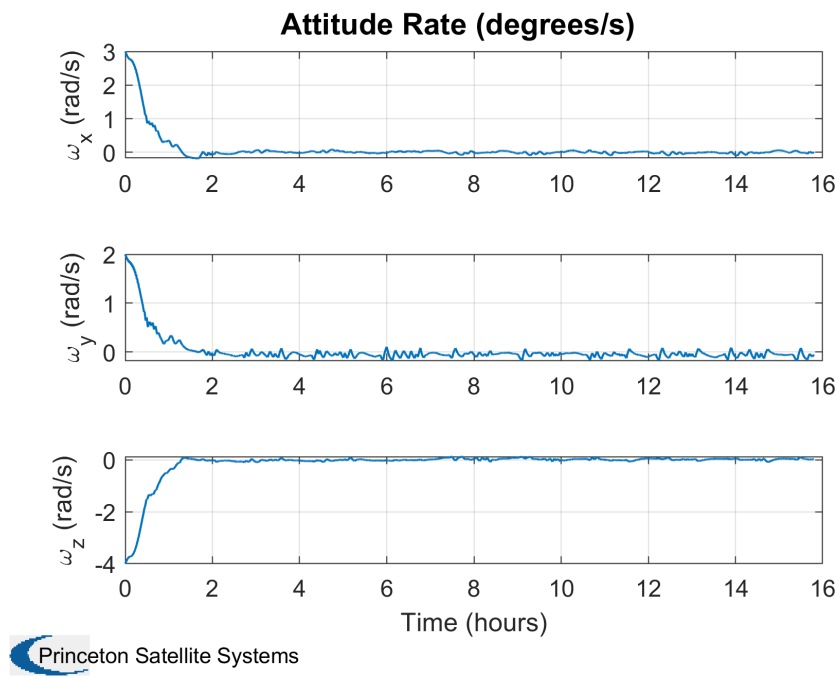


Figure 3.19: Attitude Rate

- **Generated torque**

In the pictures below it is observed the generated torque by the magnetic moment generated by the magnetorquers. This torque is the required torque to be applied in order to conduct the Nadir Pointing mode.

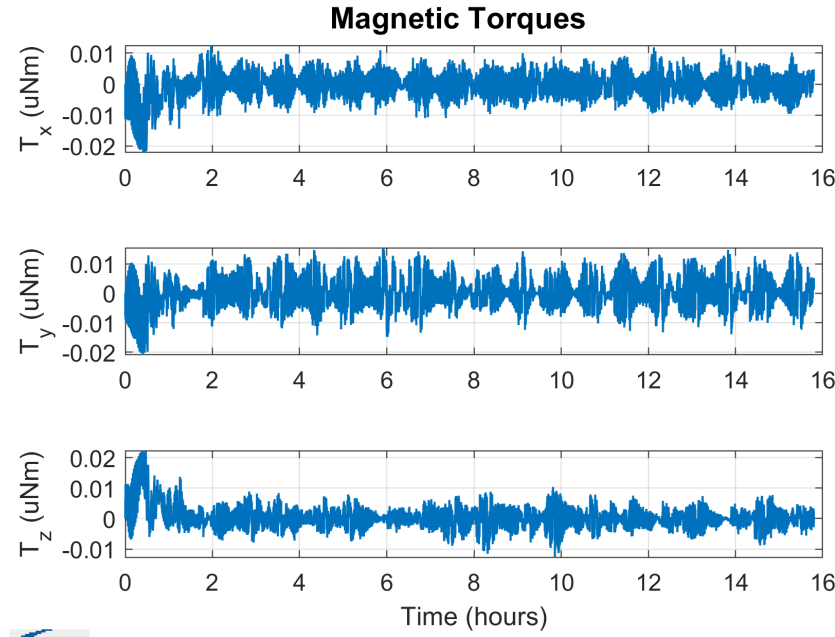


Figure 3.20: Magnetic torque

- **Injected Intensity**

The following plots show the required intensity to be injected in the magnetorquers in order to generate the necessary magnetic moment to conduct the Nadir Pointing mode. It can be observed that the intensity is quantified due to the limitations of the magnetorquer driver, as it can only inject from 0.5 mA to 32 mA in steps of 0.5 mA. If the computed intensity exceeds the maximum value, the simulation limits this intensity to 32 mA, as can be seen in the first hour of the simulation.

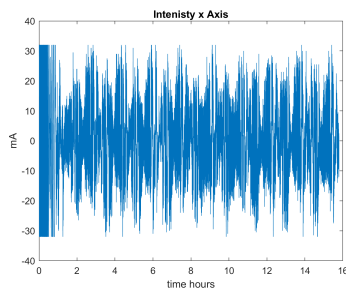


Figure 3.21: Intensity x Axis

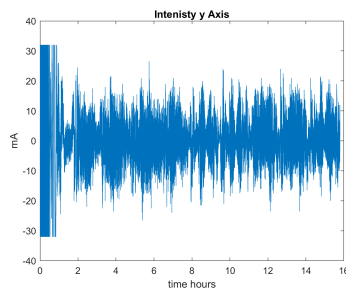


Figure 3.22: Intensity y Axis

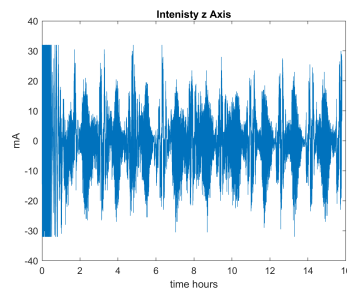


Figure 3.23: Intensity z Axis

- **Attitude quaternion**

The following plot indicates the attitude quaternion of the PQ. The selected quaternion is the one representing the rotation from the LVLH frame to the body frame. This quaternion is selected to show the performance of the Nadir Pointing mode, as the quaternion indicating that the PQ is pointing to the Nadir angle has a very simple representation, which is the quaternion $[+1, 0, 0, 0]$. In the plot can be observed that the scalar component (q_s) of the quaternion of the PQ is the desired one. Nevertheless, the vectorial part is where can be observed the effect of the noise of the sensors and the errors in the estimations, they do not converge exactly to zero; instead, residual errors remain, resulting in some inaccuracy in the pointing.

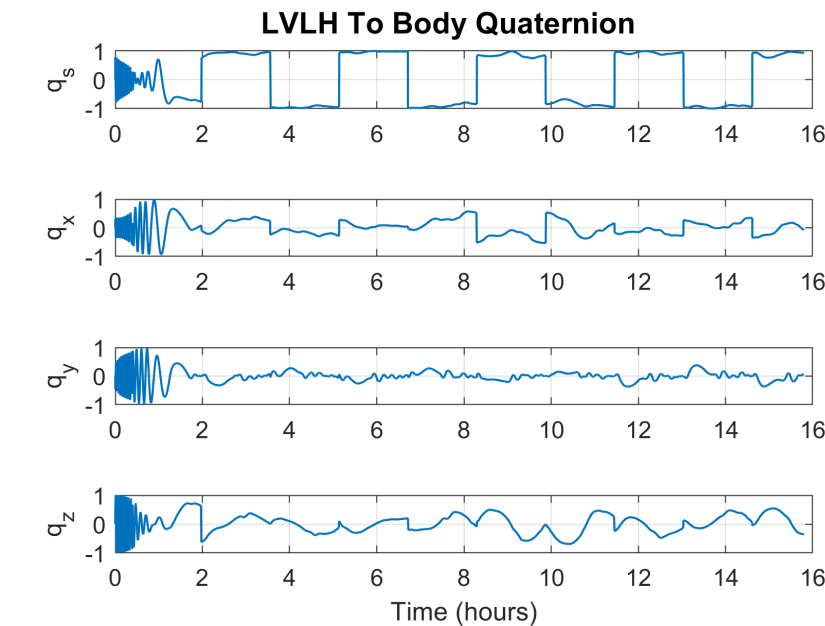


Figure 3.24: LVLH To Body Quaternion

In the picture below can be observed the APE of the Payload, which is the angle between the nadir vector and the +Y unitary vector of the body frame. Additionally, there is a line marking the 20° limit, which is the requirement of the Nadir Pointing mode. Overall, the results show that the requirement is not met, therefore, a solution to improve the performance has to be implemented. The proposed solution is the implementation of an Extended Kalman Filter (EKF) to improve the attitude estimation, which will be presented in the next section.

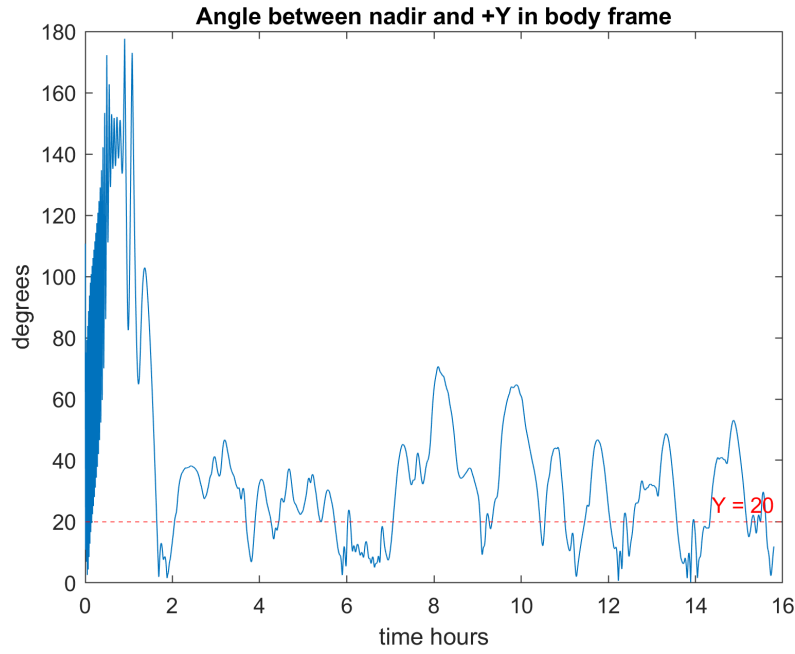


Figure 3.25: Angle between nadir and +Y

If the delay of 1 cycle of AOCS is implemented, the final result of the APE is shown below.

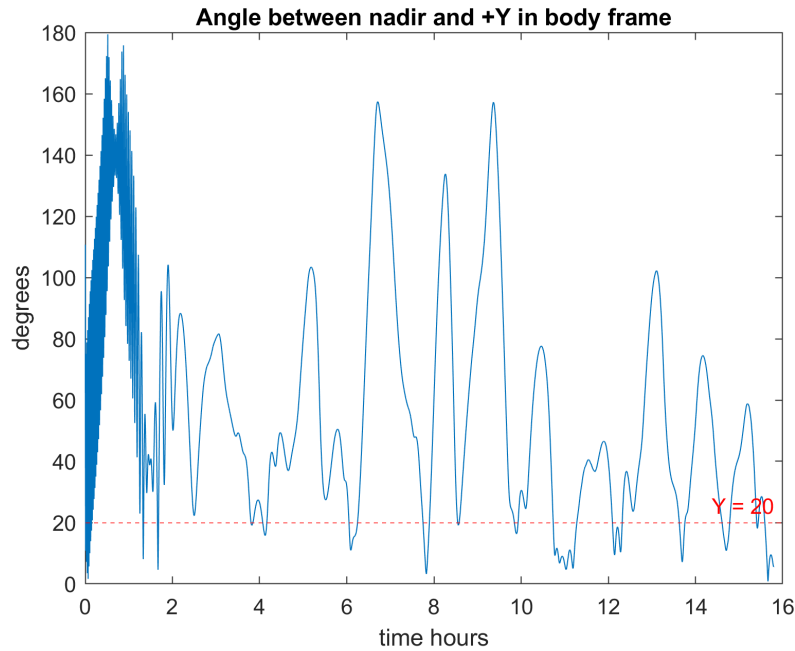


Figure 3.26: Angle between nadir and +Y with delay

As can be seen the Nadir pointing with the delay of 1 AOCS cycle does also not meet the requirement of the APE so the implementation of the EKF is compulsory.

3.1.3 Nadir pointing using an Extended Kalman Filter (EKF) for attitude determination

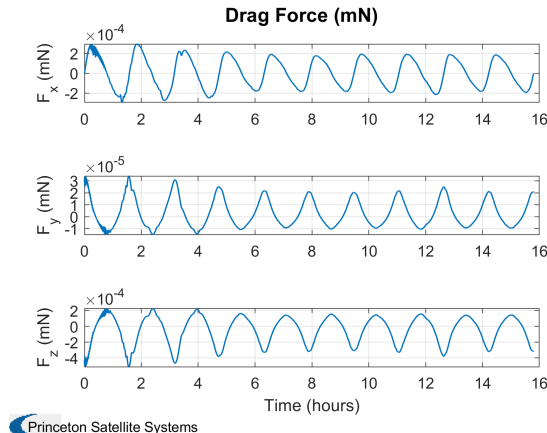
In consequence of the results obtained in the previous seconds, the proposed solution to achieve the requirement of the Payload is to implement an EKF to improve the attitude estimation. The EKF used is the one proposed in [5]. This proposed EKF uses the manifold theory to update the attitude quaternion, the covarianve matrix of the state

and the angular velocity. Additionally, it uses measurements from the gyroscope and the magnetometer to update the state of the EKF.

In this section the results of the simulation of the Nadir Pointing using the EKF are presented, including in all the results a delay of 1 AOCS cycle. In addition, the performance of the EKF is analysed and compared with the performance of the Nadir Pointing mode without the EKF.

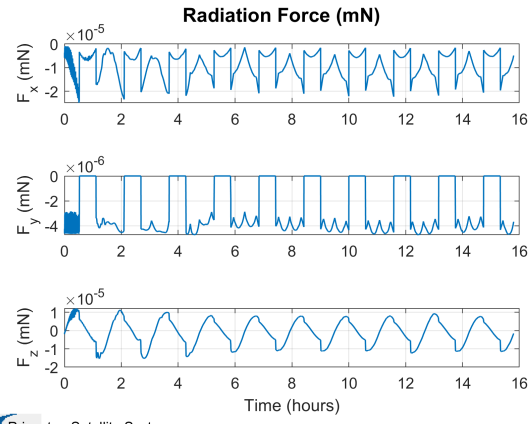
- **External perturbations**

In this section all the external perturbations affecting the PQ are presented.



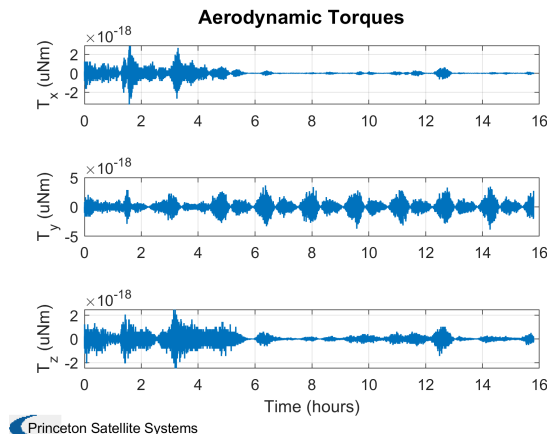
Princeton Satellite Systems

Figure 3.27: Drag Force (mN)



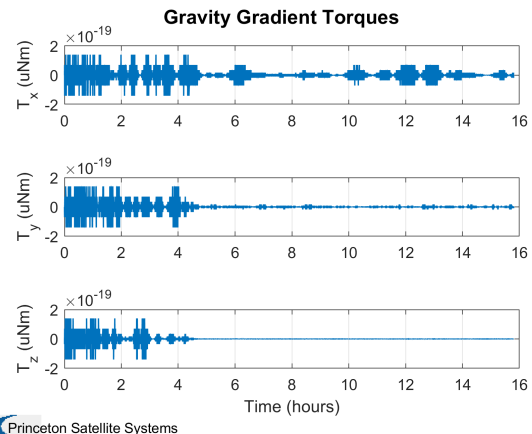
Princeton Satellite Systems

Figure 3.28: Radiation Force (mN)



Princeton Satellite Systems

Figure 3.29: Aerodynamic Torques



Princeton Satellite Systems

Figure 3.30: Gravity Gradient Torques

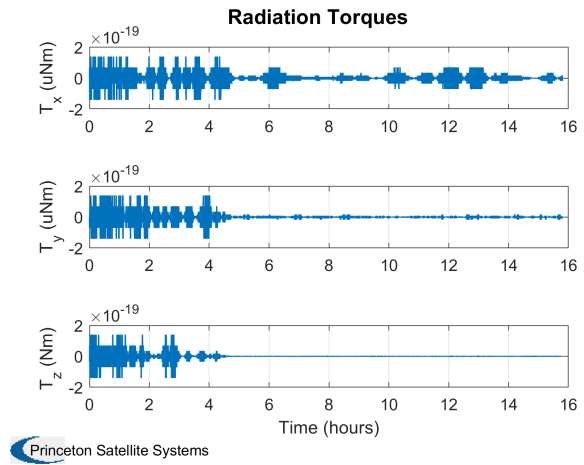


Figure 3.31: Radiation Torques

- **Sensor measurements**

In this section a s in the previous simulation, the sensor measurements are presented. Firstly, the gyroscope measurements are shown.

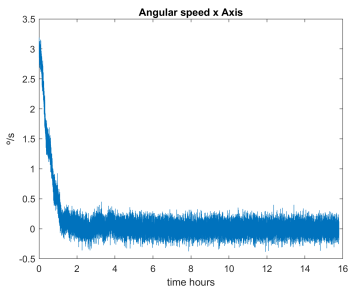


Figure 3.32: Gyro data X Axis

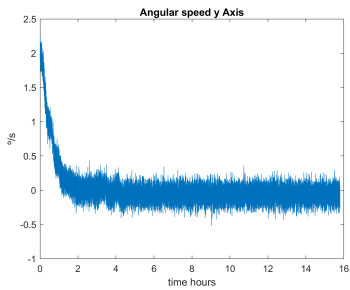


Figure 3.33: Gyro data Y Axis

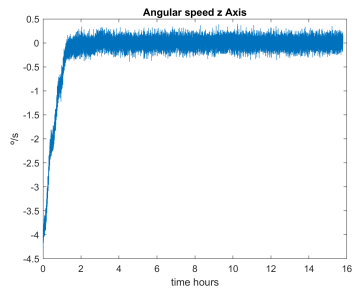


Figure 3.34: Gyro data Z Axis

Secondly, the magnetometer measurements are presented.

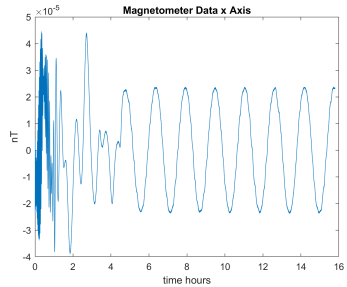


Figure 3.35: Magnetometer data X Axis

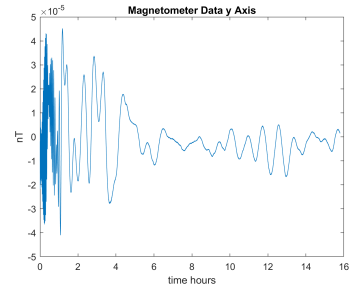


Figure 3.36: Magnetometer data Y Axis

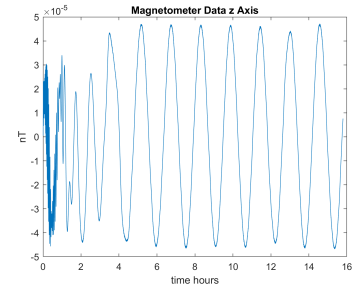


Figure 3.37: Magnetometer data Z Axis

Finally, the photodiode measurements are presented. As in the previous simulation, each axis of the PQ corresponds to the following number: 1 to +Z, 2 to -Z, 3 to +X, 4 to +Y, 5 to -X and 6 to -Y.

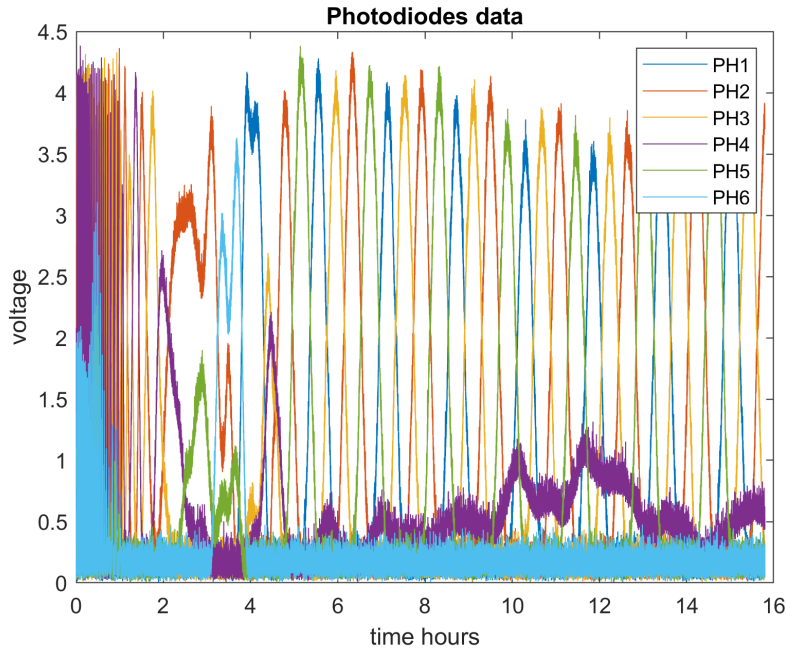


Figure 3.38: Photodiode data

- **Sun Position Algorithm Performance**

In this section the performance of the developed Sun position algorithm estimator that uses the photodiodes and the temperature sensors is presented. Remember that the orange line indicates the real position of the sun, and the blue line indicates the estimation of the algorithm.

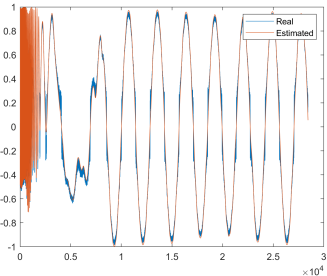


Figure 3.39: Sun position (ECI) X Axis

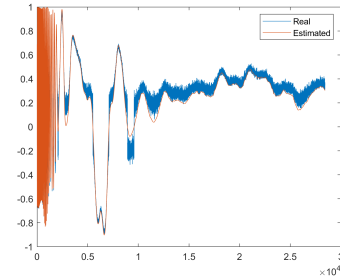


Figure 3.40: Sun position (ECI) Y Axis

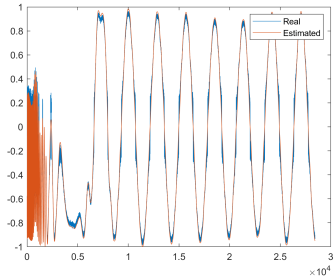


Figure 3.41: Sun position (ECI) Z Axis

- **Real angular Velocity**

This section presents the angular velocity propagated in each iteration of the simulation.

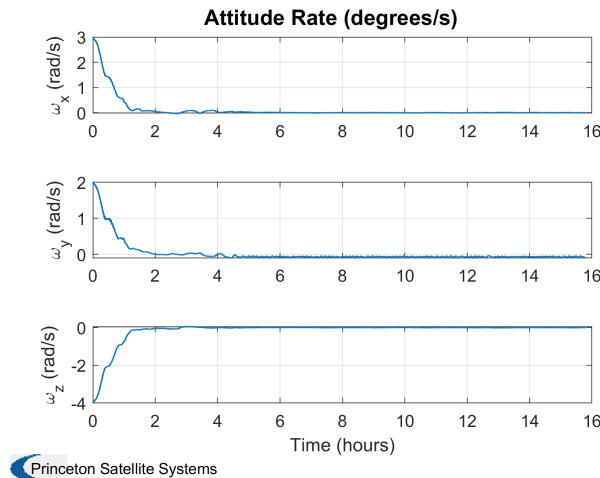


Figure 3.42: Attitude Rate

- **Generated torque**

The following plot shows the generated torque by the magnetic moment generated by the magnetorquers.

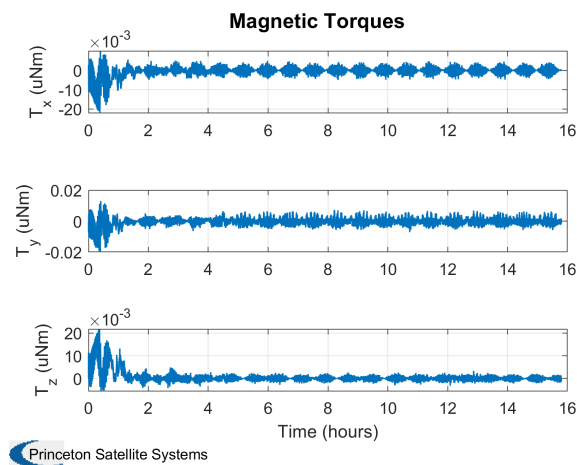


Figure 3.43: Magnetic Torques

- **Injected Intensity**

This section illustrates the required intensity to be injected in the magnetorquers in order to generate the necessary magnetic moment to conduct the Nadir Pointing mode.

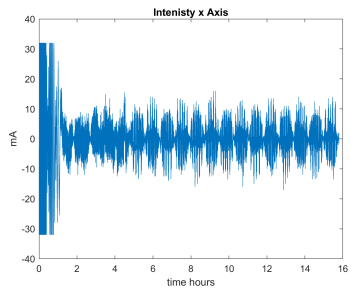


Figure 3.44: Intensity x Axis

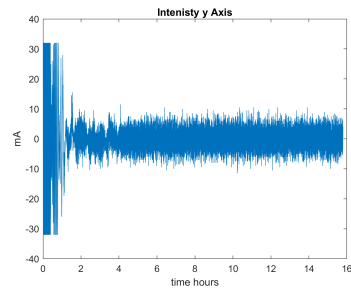


Figure 3.45: Intensity y Axis

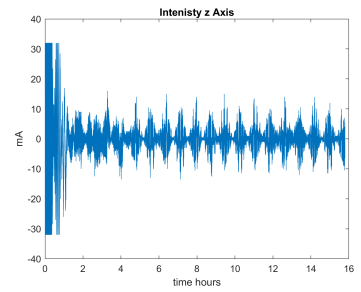
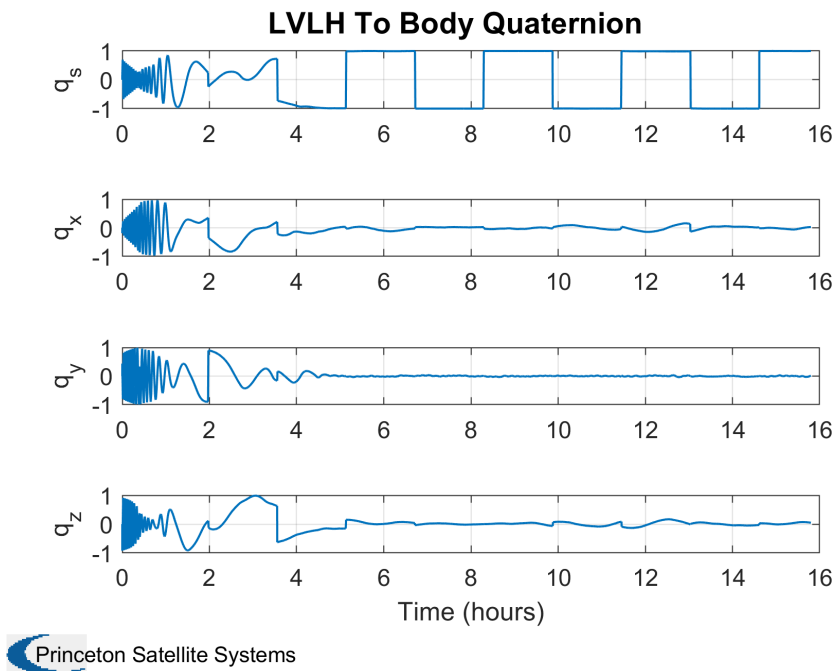


Figure 3.46: Intensity z Axis

- **Attitude quaternion**

In this section the attitude quaternion of the PQ estimated by the EKF is presented. A comparative between

the quaternion estimated by the EKF and the quaternion estimated by the simulation without the EKF will be presented in later sections.



 Princeton Satellite Systems

Figure 3.47: LVLH To Body Quaternion

The picture below shows the APE of the nadir pointing, as can be observed the performance increases significantly and now it is compliant with the requirement set by the payload.

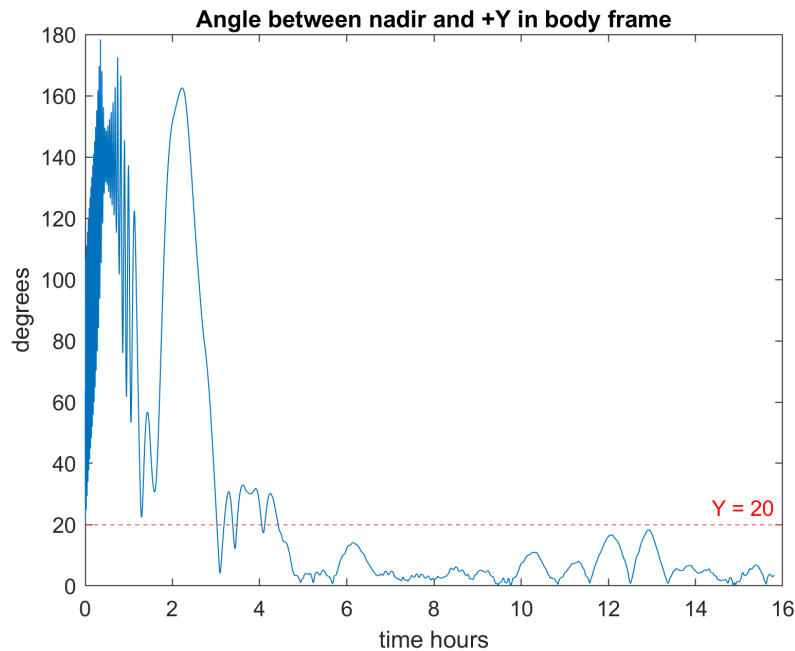


Figure 3.48: LVLH To Body Quaternion

In the picture below it can be observed the effect of the delay of 1 AOCS cycle in the APE of the nadir pointing. As can be seen, the performance is still compliant with the requirement set by the payload, but the time it needs to converge is longer than without the delay.

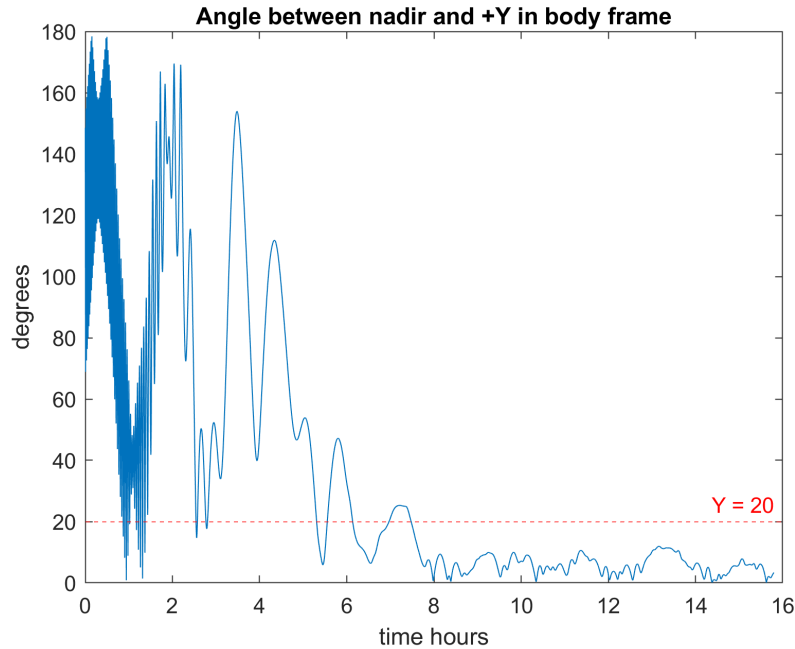


Figure 3.49: LVLH To Body Quaternion

- **EKF Performance**

To assess the performance of the EKF, a performance campaign has been conducted. The campaign consists of 20 simulations using the same initial state and orientation of the PQ. After each simulation the orientation of the PQ is extracted by means of the quaternion describing the rotation from the LVLH frame to the body frame. Finally that quaternion is used to calculate the mean square error (MSE) of each quaternion component, so that the performance of the EKF can be evaluated. In order to compute the MSE, the ideal quaternion used is the quaternion $[1, 0, 0, 0]$, which represents the ideal attitude of the PQ in the Nadir Pointing mode.

The first plot shows the quaternion evolution for the 20 simulations, where it can be observed that in overall, all the quaternion components manage to converge approximately to the ideal quaternion.

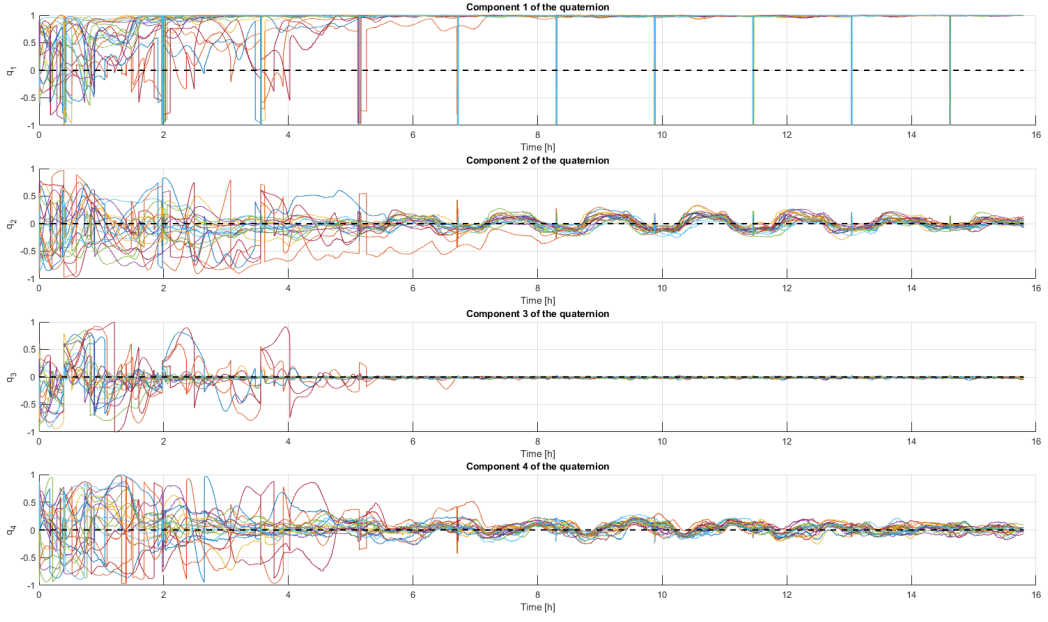


Figure 3.50: Quaternion evolution for 20 simulations

The following plots show the MSE of each quaternion component. Additionally, the bias², the variance and the first component of the covariance matrix are also presented.

In the first plot, the component q_1 of the quaternion is presented, which is the scalar component of the quaternion. In this case, it can be observed that overall the MSE is very low, which indicates that the EKF is able to estimate the scalar component of the quaternion in a very accurate way.

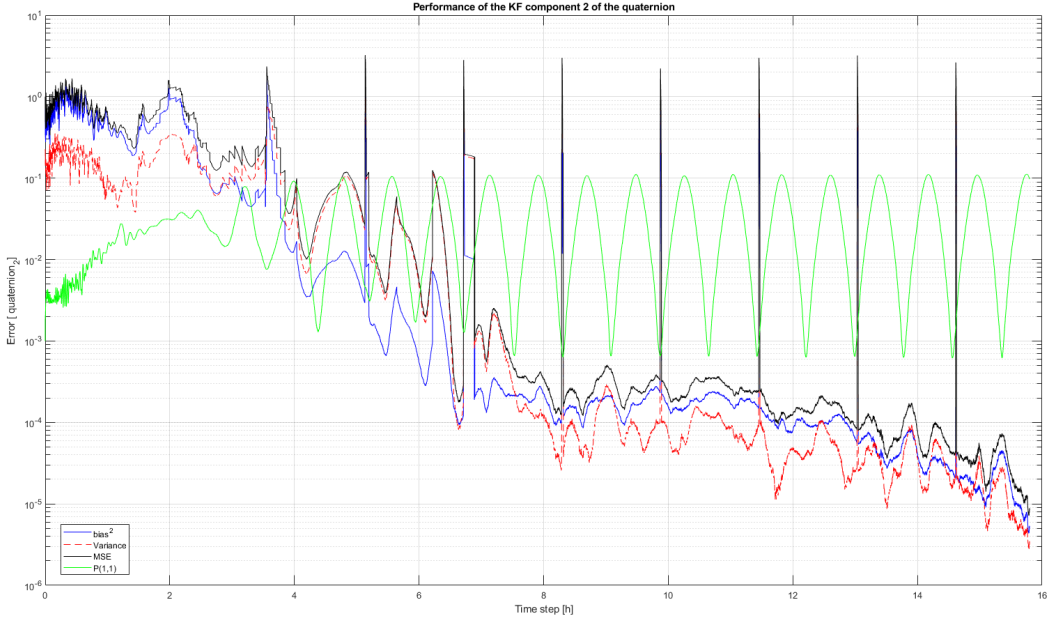


Figure 3.51: Performance q_1

In the following three plots, the components q_2 , q_3 and q_4 of the quaternion are presented. In this case these components are more valuable for obtaining a better nadir pointing performance. Firstly, in all plots can be

observed two different phases, on the one hand, the first phase in which the EKF tries to reduce the angular velocity to 0 and tries to point as close as possible to the nadir vector. In this phase the EKF as can be seen works as the optimal estimator, as the variance is very close to the MSE. This happens because the EKF detects that the covariance matrix variates in time, thus the EKF tries to reduce the MSE and as a consequence the variance to achieve a more constant covariance matrix. In order to do that, the EKF assigns more confidence in the measurements than in the predictions.

In the second phase, once the angular velocity has been significantly reduced and the attitude has converged near the nadir direction, the EKF enters a tracking or steady-state phase. At this point, the estimation no longer requires aggressive corrections. This is reflected in the covariance matrix, which becomes more stable and varies less over time. Since the EKF assumes the system is already well-aligned with the nadir direction, it relies more heavily on its predictions rather than the incoming measurements.

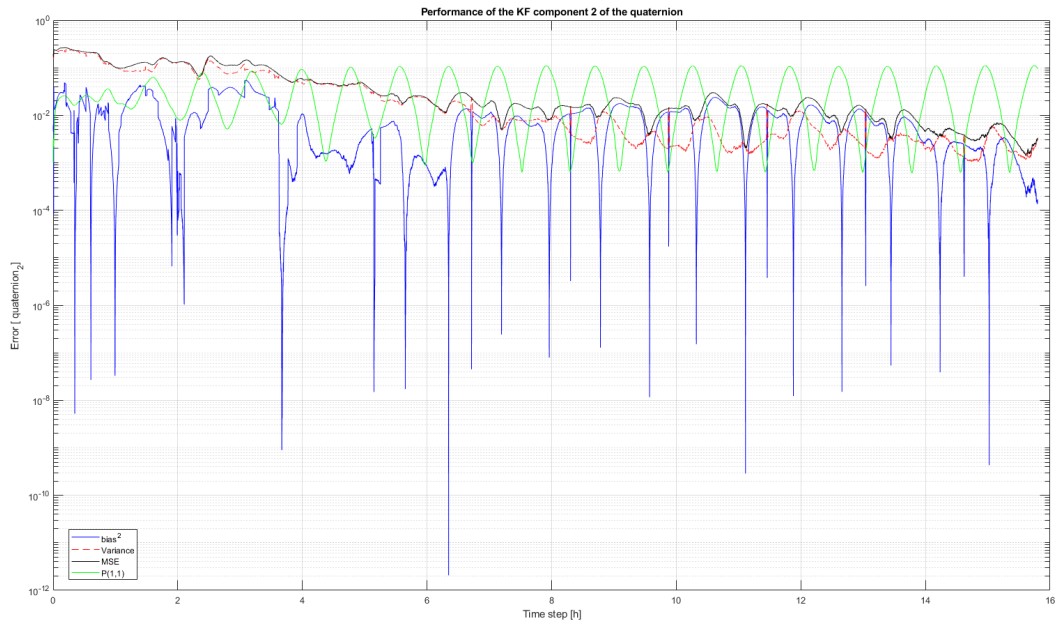


Figure 3.52: Performance q_2

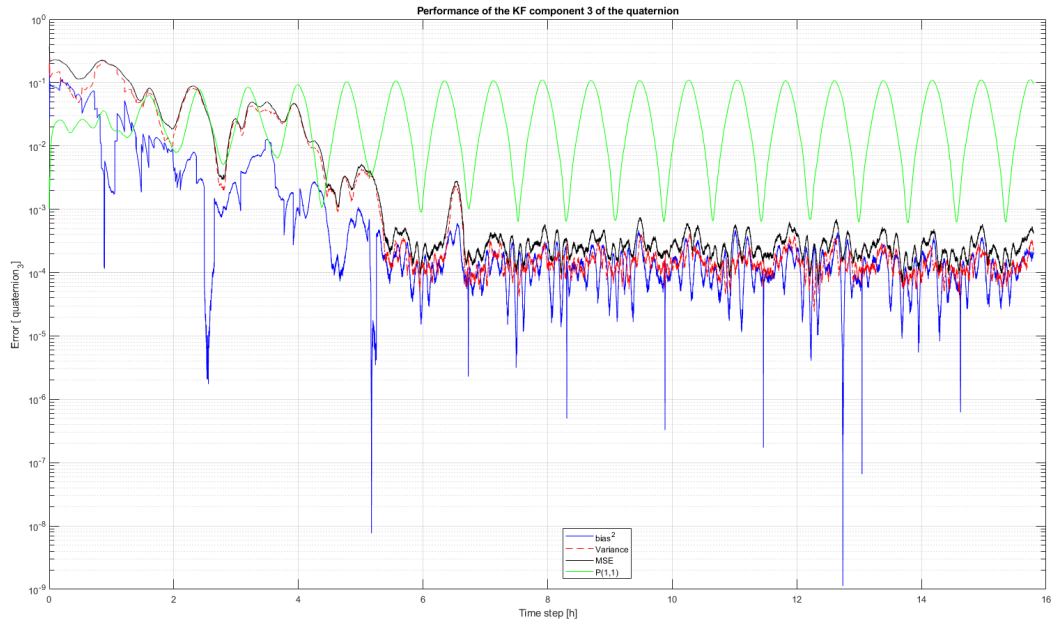


Figure 3.53: Performance q_3

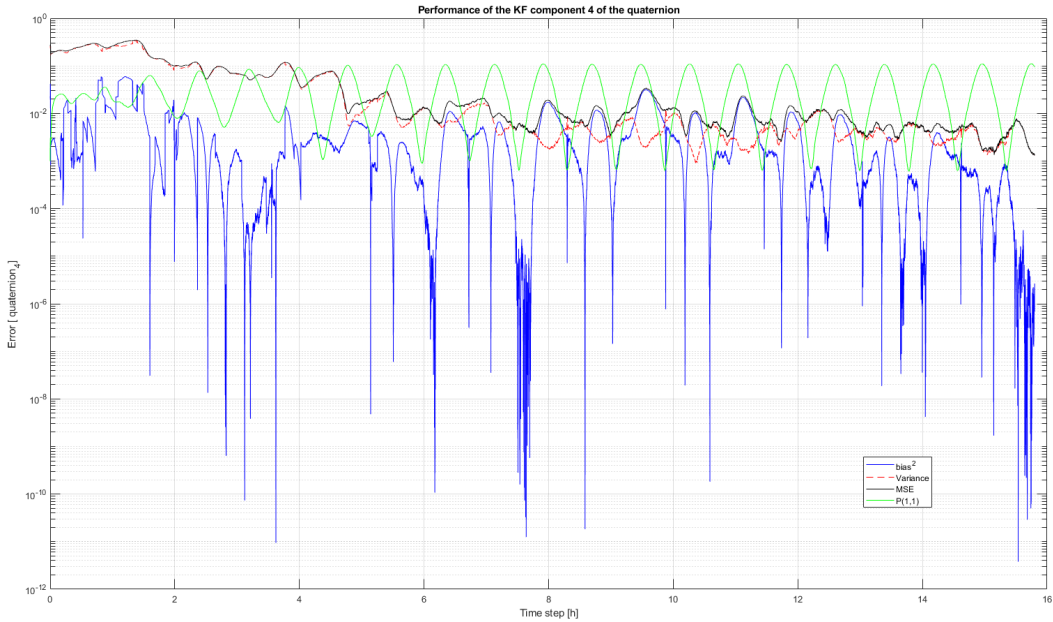


Figure 3.54: Performance q_4

3.2 Detumbling mode

References

- [1] Princeton University. Created toolboxes. <https://psatellite.com/>, 2017.
- [2] Wikipedia. Dipole model of the Earth's magnetic field. https://en.wikipedia.org/wiki/Dipole_model_of_the_Earth%27s_magnetic_field, 2025.
- [3] Johnson,D.L and Smith, R.E. The MSFC/J70 orbital atmosphere model and the data bases for the MSFC solar activity prediction technique. <https://ntrs.nasa.gov/citations/19860012552>, 1985.
- [4] F. L. Markley and J. L. Crassidis,. Fundamentals of Spacecraft Attitude Determination and Control, 2014.
- [5] Bernal-Polo, P.; Martínez-Barberá,. Kalman Filtering for Attitude Estimation with Quaternions and Concepts from Manifold Theory. <https://doi.org/10.3390/s19010149>, 2019.